RAPID COMMUNICATION

Electronic structure and spatial inhomogeneity of iron-based superconductor FeS*

Chengwei Wang(王成玮)[1,2,3,†], Meixiao Wang(王美晓)[2,†], Juan Jiang(姜娟)[2,4,†], Haifeng Yang(杨海峰)[2], Lexian Yang(杨乐仙)[5], Wujun Shi(史武军)[2], Xiaofang Lai(赖晓芳)[6], Sung-Kwan Mo[4], Alexei Barinov[7], Binghai Yan(颜丙海)[8], Zhi Liu(刘志)[1,2], Fuqiang Huang(黄富强)[6,9], Jinfeng Jia(贾金峰)[10], Zhongkai Liu(柳仲楷)[2,‡], and Yulin Chen(陈宇林)[2,5,11,§]

[1] *State Key Laboratory of Functional Materials for Informatics, Shanghai Institute of Microsystem and Information Technology (SIMIT), Chinese Academy of Sciences, Shanghai* 200050, *China*

[2] *School of Physical Science and Technology, ShanghaiTech University, CAS-Shanghai Science Research Center, Shanghai* 200031, *China*

[3] *University of Chinese Academic of Sciences, Beijing* 100049, *China*

[4] *Advanced Light Source, Lawrence Berkeley National Laboratory, Berkeley, CA* 94720, *USA*

[5] *State Key Laboratory of Low Dimensional Quantum Physics, Department of Physics and Collaborative Innovation Center for Quantum Matter,Tsinghua University, Beijing* 100084, *China*

[6] *Beijing National Laboratory for Molecular Sciences and State Key Laboratory of Rare Earth Materials Chemistry and Applications, College of Chemistry and Molecular Engineering, Peking University, Beijing* 100871, *China*

[7] *Elettra-Sincrotrone Trieste ScPA, Trieste, Basovizza* 34149, *Italy*

[8] *Max Planck Institute for Chemical Physics of Solids, D*-01187 *Dresden, Germany*

[9] *State Key Laboratory of High Performance Ceramics and Superfine Microstructure, Shanghai Institute of Ceramics, Chinese Academy of Sciences, Shanghai* 200050, *China*

[10] *Key Laboratory of Artificial Structures and Quantum Control (Ministry of Education), Department of Physics and Astronomy, Shanghai Jiao Tong University, Shanghai* 200240, *China*

[11] *Physics Department, Oxford University, Oxford, OX*1 3*PU, UK*

(Received 31 December 2019; revised manuscript received 1 February 2020; accepted manuscript online 13 February 2020)

Iron-based superconductor family FeX (X = S, Se, Te) has been one of the research foci in physics and material science due to their record-breaking superconducting temperature (FeSe film) and rich physical phenomena. Recently, FeS, the least studied FeX compound (due to the difficulty in synthesizing high quality macroscopic crystals) attracted much attention because of its puzzling superconducting pairing symmetry. In this work, combining scanning tunneling microscopy and angle resolved photoemission spectroscopy (ARPES) with sub-micron spatial resolution, we investigate the intrinsic electronic structures of superconducting FeS from individual single crystalline domains. Unlike FeTe or FeSe, FeS remains identical tetragonal structure from room temperature down to 5 K, and the band structures observed can be well reproduced by our *ab-initio* calculations. Remarkably, mixed with the 1×1 tetragonal metallic phase, we also observe the coexistence of $\sqrt{5} \times \sqrt{5}$ reconstructed insulating phase in the crystal, which not only helps explain the unusual properties of FeS, but also demonstrates the importance of using spatially resolved experimental tools in the study of this compound.

Keywords: angle-resolved photoemission with spatially resolution, scanning tunneling microscopy, iron-based superconductor, electronic band structure

PACS: 74.25.Jb, 71.27.+a **DOI:** 10.1088/1674-1056/ab75d4

In the past few years, Fe-based superconductors (FeSCs) have been intensively studied due to their rich and unusual properties, such as multi-orbital band character,[1] close relation to magnetism,[2] intermediate correlation level,[3] and complex pairing mechanism,[4] which make FeSCs rich yet intriguing systems for the understanding of high temperature superconductivity.[5,6] Among FeSCs, the iron chalcogenide family compounds FeX (X = S, Se, Te) have attracted enormous research interests recently due to their simple crystal structure, relatively strong correlation,[3,7] and the highest superconducting transition temperature (T_c) among all FeSCs (thin film FeSe, see Refs. [8–10]).

Despite the theoretical calculations that predicted similar electronic structures for all FeX compounds,[11] their physi-

*Project supported by CAS-Shanghai Science Research Center, China (Grant No. CAS-SSRC-YH-2015-01), the National Key R&D Program of China (Grant No. 2017YFA0305400), the National Natural Science Foundation of China (Grant Nos. 11674229, 11227902, and 11604207), the EPSRC Platform Grant (Grant No. EP/M020517/1), Hefei Science Center, Chinese Academy of Sciences (Grant No. 2015HSC-UE013), Science and Technology Commission of Shanghai Municipality, China (Grant No. 14520722100), and the Strategic Priority Research Program (B) of the Chinese Academy of Sciences (Grant No. XDB04040200).

†These authors contributed equally to this work.

‡Corresponding author. E-mail: liuzhk@shanghaitech.edu.cn

§Corresponding author. E-mail: yulin.chen@physics.ox.ac.uk

cal properties show dramatic differences: while FeTe is non-superconducting, possesses an antiferromagnetic ground state below ~ 75 K with a large magnetic moment ($\sim 2.4\ \mu_B$/Fe), and exhibits strong electron correlations,[12–15] FeSe superconducts ($T_c \sim 8$ K for the bulk crystal[16] and ~ 65 K for the monolayer film on $SrTiO_3$[8–10]) and the superconductivity coexists with a nematic phase in the orthorhombic lattice (C_2 symmetry) at low temperature which becomes tetragonal (C_4 symmetry) above ~ 90 K.[17,18] FeS, the main focus of this work, also superconducts ($T_c = 4.5$ K for the bulk crystal) with a tetragonal crystal structure, but without magnetic order[19,20] or phase transition to orthorhombic lattice. These differences from both FeTe and FeSe make it important to explore the electronic structure of FeS in order to understand the mechanism of superconductivity in the FeX family, as well as the coexistence or competition of the superconducting order with other degrees of freedom (e.g., lattice and magnetism).

Unlike the numerous studies of FeTe and FeSe, up to date, the electronic structure of FeS still awaits experimental investigation, partially due to the difficulty in the synthesis of high quality macroscopic single crystalline samples, as FeS is usually prepared by iron corrosion or co-precipitation methods and thus is very reactive toward oxygen and tends to transform into other iron sulphide phases.[21–23] Recently, high quality single crystals of FeS were successfully synthesized by mild hydrothermal reaction, and the bulk crystals superconducted at ~ 4.5 K.[19,24] Remarkably, recent thermal conductivity and specific heat measurements suggested a nodal superconducting gap structure in FeS,[25] making the mechanism of the superconductivity in the FeX family elusive. Under this circumstance, the investigation on the electronic structures of FeS is urged, which, together with the comparison to those of FeTe and FeSe, will greatly help comprehend the unusual superconductivity in FeX family compounds.

Although the crystal quality of FeS has been significantly improved by hydrothermal reaction, the typical single crystalline domain size is of tens of micrometers, less than the typical beamspot size (hundreds of micrometers) of most conventional angle resolved photoemission spectroscopy (ARPES) setups, posing a great difficulty for the direct investigation of its electronic structure. In this letter, in addition to conventional ARPES, we further utilize the state-of-the-art spatially resolved ARPES with sub-micrometer resolution (μ-ARPES) and scanning tunneling microscopy (STM) to systematically investigate the electronic structure and spatial inhomogeneity of superconducting FeS single crystals. Our results clearly reveal the detailed topographic and electronic structure of FeS, showing clear $C4$ symmetry with multiple hole- and electron-pockets around the $\overline{\Gamma}$ and $\overline{M}$ points in its Fermi-surface, consistent with our *ab-initio* calculations. Interestingly, although the tetragonal phase and the associated electronic structures of FeS resemble those of FeTe and FeSe at high temperature; no tetragonal to orthorhombic phase transition is observed in FeS in a stark contrast to FeSe. This suggests a pure superconducting ground state in FeS and makes it a unique case among all the FeX compounds. Also remarkably, in addition to the metallic (tetragonal) phase, our μ-ARPES and STM measurements further identify a coexisting $\sqrt{5} \times \sqrt{5}$ reconstructed insulating phase in the crystal, which should be considered for the comprehensive understanding of the unusual properties in different measurements on macroscopic FeS crystals (such as sample-to-sample variations in magnetism observed in the μSR measurement[26]).

The FeS crystals are prepared by hydrothermally extracting potassium atoms from parent material $K_{0.8}Fe_{1.6}S_2$ synthesized in self-flux method[19] (see supplementary information for details). Figure 1(a) shows a tetragonal lattice structure of FeS composed of stacking edge-sharing FeS_4-tetrahedra with S atoms siting above and below the Fe plane ($P4/nmm$ space group), similar to other FeX in their tetragonal phase. The interaction between the FeS layers is weak, thus flat terrace structures could be observed in the synthesized FeS single crystals (see the SEM image in the inset of Fig. 1(b)). The tetragonal structure of FeS has been demonstrated by the x-ray diffraction (XRD) pattern at room temperature (300 K, Fig. 1(b)) and STM measurements at low temperature (~ 5 K) with atomic resolution (Fig. 1(c) and supplementary information). The fast-Fourier transformation (FFT) of the STM measurements in Fig. 1(c) clearly identifies the lattice constant as $a = b = 3.681$ Å, confirming the tetragonal lattice structure of FeS at low temperature (Fig. 1(d)). In addition, the STM topographic image in Fig. 1(c) shows multiple dumbbell shaped defects centered at the Fe atom sites (similar to the previous report in FeS[27] and FeSe[28–31]) that result from the substitution of Fe atoms by the excess S or alkali atoms (Na or K) during the crystal synthesis. The high quality of the FeS single crystal is also demonstrated by the sharp superconducting transition (Fig. 1(e)) and large superconducting volume (Fig. 1(f)) obtained from the resistivity and magnetic susceptibility measurements, respectively. From room temperature down to T_c, FeS behaves metallic and does not experience a structural phase transition (Figs. 1(b)–1(f)), making it a unique case among the FeX family compounds.

We first investigate the general electronic structure of FeS by conventional ARPES (beamspot size is ~ 100 μm). From the Fermi surface (FS) map (Fig. 2(a)(i)), we can identify pockets around the $\overline{\Gamma}$ and $\overline{M}$ points (the high symmetry points are defined in the 2-Fe BZ). From the dispersions along the high symmetry $\overline{M}$–$\overline{\Gamma}$–$\overline{M}$ direction (Fig. 2(a)(ii)), it is clear that the pocket at $\overline{\Gamma}$ is hole-like and those at $\overline{M}$ are electron-like. The observed band structure can be well reproduced by our *ab-initio* calculations (Fig. 2(b)), where there are two hole/electron bands cross E_F around $\overline{\Gamma}/\overline{M}$, respectively. The

two bands' crossing can be experimentally seen by polarizations measurements, as the total ARPES intensity depends on the transition matrix elements,[32] the photoemission intensity of the odd parity d_{xz} bands around $\overline{\Gamma}$ is enhanced/suppressed with photon polarization perpendicular/parallel to the crystal mirror plane (Fig. 2(c)(i)); while the effect is opposite for the even parity d_{yz} bands (Fig. 2(c)(ii)).[32–34] We can thus use the linear horizontal (LH) and linear vertical (LV) polarization photons to selectively probe the d_{xz} and d_{yz} bands, respectively, as can be seen in Figs. 2(c)(i) and Fig. 2(c)(ii), respectively. In addition, the ARPES results also agree well with the STM measurements, as in Fig. 2(c)(iv), the integrated ARPES energy distribution curve (EDC) over the whole Brillouin zone (BZ) shows nice agreement with the dI/dV curve from our STM measurement (Fig. 2(c)(iv)), as both reflect the total density of state (DOS) from different bands of FeS.

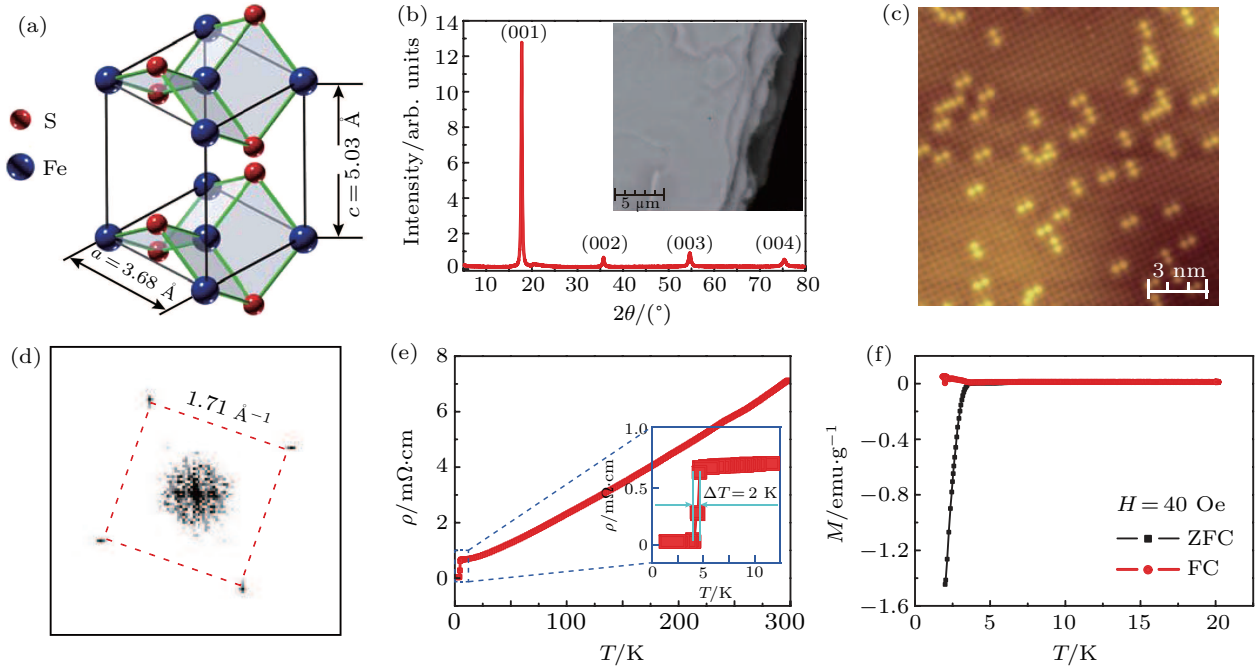

Fig. 1. Physical properties of hydrothermally synthesized FeS. (a) Crystal structure of layered tetragonal FeS. (b) XRD pattern and SEM image of FeS measured at room temperature. (c) STM topography image of FeS measured at ∼ 5 K. Dumb-bell-shape bright spots are defects from excess S or alkali metals from the synthesis process. (d) FFT of (c) shows four spots forming a square. (e) Resistivity versus temperature curve. The inset shows the superconducting transition with $\Delta T = 2$ K. (f) Magnetic susceptibility versus temperature measured under a magnetic field of 40 Oe, in both zero-field-cooling (ZFC) and field-cooling (FC) processes.

The observed electronic structure of FeS shares broad similarities with other iron chalcogenides in their high-temperature tetragonal phase,[35–37] such as the number of hole bands/pockets around $\overline{\Gamma}$ and electron bands/pockets around $\overline{M}$, and the orbital dependent enhancement of the effective mass (the effective mass renormalization factor is ~ 2 for the d_{xz} and d_{yz} bands and ~ 3.5 for the d_{xy} band; and the large renormalization of the d_{xy} band makes the bottom of the d_{xy} band sit above the d_{xz} hole band, similar to that in FeSe).

However, unlike FeSe or FeTe, the tetragonal crystal and electronic structures of FeS persist at low temperature (~ 5 K); while at low temperature ($T <\sim 90$ K), FeSe shows two-fold orthorhombic symmetry,[29,35] and FeTe enters the antiferromagnetic state with large magnetic moment (when $T <\sim 75$ K), leading to strong electron correlation and mode coupling (i.e., polarons[14]). Therefore, FeS represents the simplest and cleanest system among all FeX compounds, thus could serve as the best model system for the investigation of the superconducting mechanism in iron chalcogenides.

It is notable that in Fig. 2, the band dispersions and the FS map appear broad and while we were able to use different photon polarizations to enhance the bands with different symmetry, the geometry, such as the FS pockets shape, remains blurry without details. This is due to the fact that in the regular ARPES system, the photon beam spotsize (~ 100 μm) is significantly larger than the typical domain size (up to ~ 30 μm) of the FeS crystals. Thus, the measurements represent the average of multiple domains which inevitably results in the relatively broader band structures as we observed in Fig. 2.

To overcome this difficulty, we further performed the μ-ARPES measurements (Fig. 3(a), the spot size is ~ 0.8 μm, much smaller than the typical FeS domain size), and the results are assembled in Fig. 3 (more details can be found in the supplementary information). As can be seen in Fig. 3(b), the FeS crystal is composed of small single crystalline domains (brighter regions) ranging from a few micrometers up to tens of micrometers, which are intermediated by the darker regions of either the insulating phases (as we will discuss below) or other impurities during the sample growth.

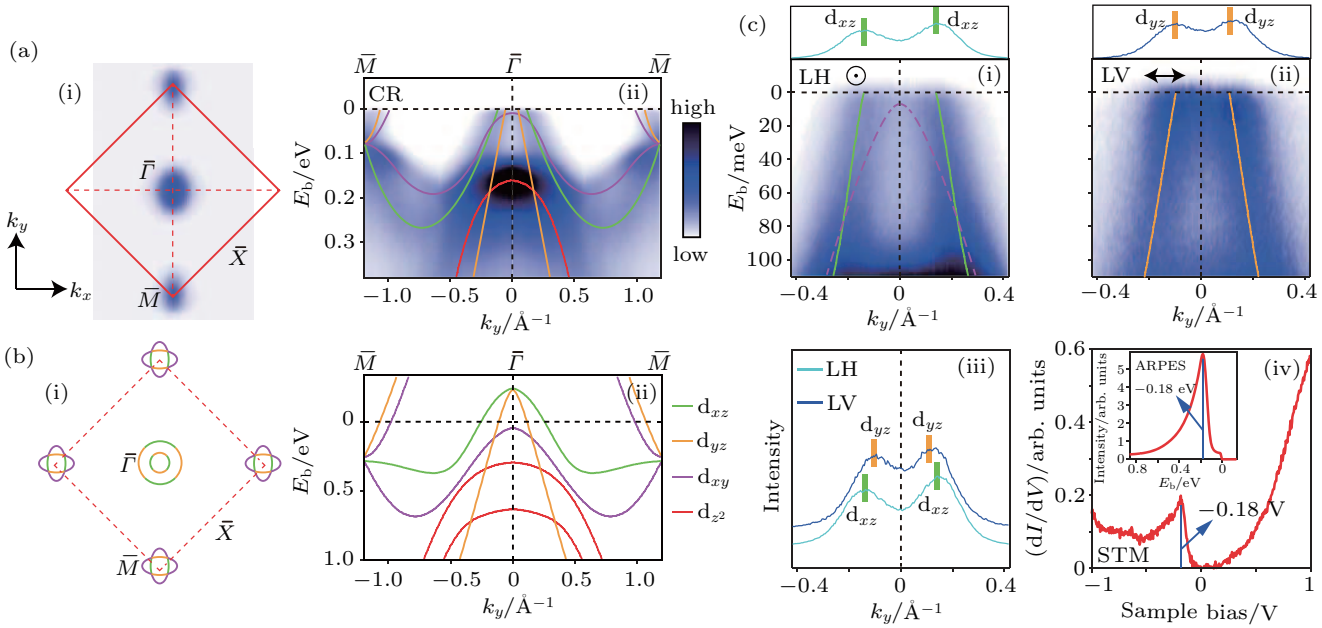

Fig. 2. General electronic structure of FeS revealed by ARPES. (a) Constant energy contour at the Fermi energy (i) and high symmetry $\bar{\Gamma}$–$\bar{M}$ cut (ii) measured with circularly right (CR) polarized light. The colored curves indicate the schematics of each band with different orbitals. (b) *Ab-initio* calculations of the Fermi surface (i) and high symmetry $\bar{M}$–$\bar{\Gamma}$–$\bar{M}$ cut (ii) of FeS. Bands with different orbital characters are plotted with different colors. (c) High symmetry $\bar{M}$–$\bar{\Gamma}$–$\bar{M}$ cut near the $\bar{\Gamma}$ point measured with linear horizontal (LH) (i) and linear vertical (LV) (ii) polarized light. The direction of polarization with respect to the cut is labeled. Colored curves represent the bands with certain orbitals that are enhanced with the polarization. The magenta dotted curve indicates the d_{xy} orbital with very weak intensity (similar to other Fe*X* compounds, see Ref. [7]). The curves on top of (i) and (ii) are the momentum distribution curves (MDCs) at the Fermi energy. The peaks from fitting each MDC are indicated, showing the positions of each band. (iii) The stack plot of the two MDCs from (i) and (ii) showing the different positions of the k_F of the d_{xz} and d_{yz} bands. (iv) Comparison plot of the dI/dV curve obtained from STM and the integrated EDC (the inset figure) from (a)(ii). All ARPES data are measured with $h\nu = 25$ eV photons at $T = 8$ K sample temperature.

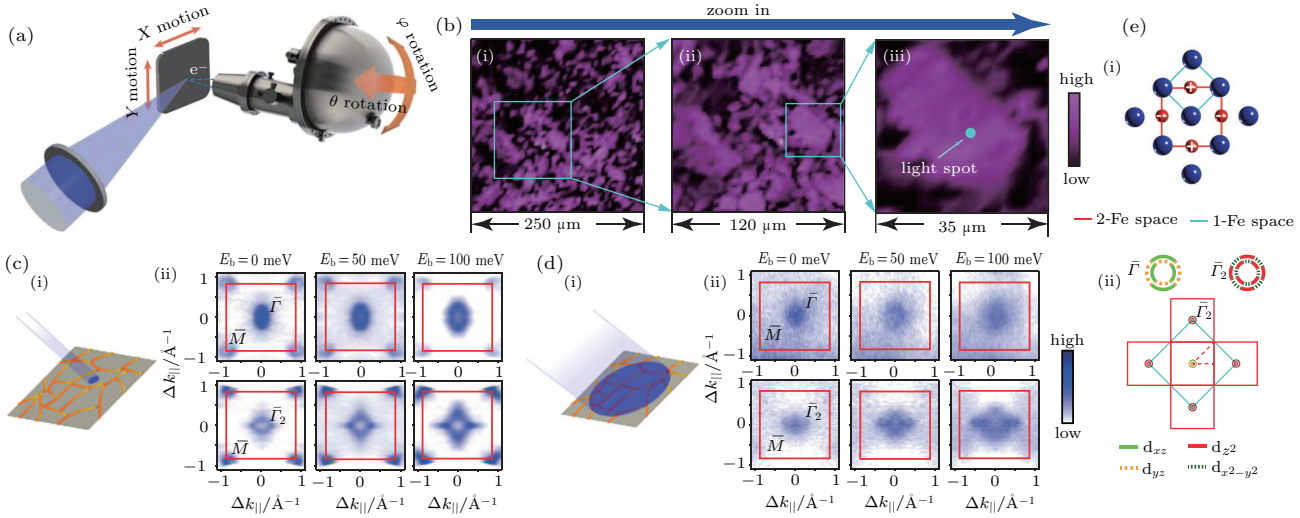

Fig. 3. Electronic structure of FeS studied by μ-ARPES. (a) Schematic diagram of the spatially resolved ARPES setup. (b) Spatial scan of FeS by μ-ARPES measuring the total photoemission intensity close to the Fermi level shows the domain size of single crystal FeS is around 35 μm×35 μm. The position and size of the beam spot during the photoemission measurement are indicated by the blue circle in (iii). (c) Constant energy contours of FeS covering the first and second BZs at various binding energies measured by μ-ARPES. (i) The schematic of the relative size of the beam spot and the FeS sample domain. (ii) The upper row plots the constant energy contours around the first $\bar{\Gamma}$ at $E_b = 0$ meV, 50 meV, and 100 meV, respectively. The lower row is the contour around the second $\bar{\Gamma}$ at the same binding energies. Data are measured with $h\nu = 74$ eV LH photons at $T = 20$ K sample temperature. (d) Same as (c), the schematic of the relative beamspot size (i) and constant contour energy plots (ii) are from the conventional ARPES setup. Data are measured with $h\nu = 180$ eV LH photons at $T = 8$ K sample temperature, (e) (i) Illustration of the 1-Fe (blue square) and 2-Fe (red square) unit-cells in FeS. The S atoms above and below the Fe plane are labeled by "+" and "−", respectively. (ii) Illustration of the 1-Fe (blue square) and 2-Fe (red square) BZs and *ab-initio* calculation of the different orbital components of the bands near the $\bar{\Gamma}$ point in the 1st and 2nd (2-Fe) BZs. Orbitals labeled with dotted curves indicate those suppressed by the measurement beam using LH polarization (see Ref. [38]).

With the sub-micrometer photon beam spot, we were able to choose a large flat domain (∼ 35 μm, see Fig. 3(b)(iii)) for the μ-ARPES measurements. Indeed, the results (Fig. 3(c)) show clear improvement over the conventional ARPES results (Fig. 3(d)), and the detailed shape of the FS pockets is now discernible — even the different shapes of the FS pockets at the $\bar{\Gamma}$ points from different BZs (Fig. 3(c)(ii)) are now clearly seen: while the FS pocket near the 1st $\bar{\Gamma}$ looks ellip-

tical, the FS pocket at the 2nd $\overline{\Gamma}$ has a cross-shape, and this difference becomes more apparent in the constant energy contours at higher binding energies (Fig. 3(c)(ii)). The different shapes of the FS pockets from different BZs can be explained by Fig. 3(e), where the orbital components of the FS pockets around the 1st and 2nd $\overline{\Gamma}$ points (Fig. 3(e)) that can be observed by ARPES are different, similar to previous ARPES studies on $FeSe_{1-x}Te_x$[38] and other iron pnictides.[39]

To understand the nature of the intermediate phase (the darker region in Fig. 3(b)), we carried out STM topographic measurements. Remarkably, in addition to the tetragonal 1×1 phase as we studied before (with lattice constant 3.6 Å, see Figs. 4(b)(i–iii), area 3), we observed well-ordered $\sqrt{5} \times \sqrt{5}$ reconstructed phase (with square unit cell and lattice constant of 8.23 Å, see Figs. 4(b)(i,ii,iv), areas 1, 2), similar to those observed in the FeSe film epitaxially grown on grapheme.[28] The $\sqrt{5} \times \sqrt{5}$ reconstruct areas in FeS are typically tens of nano-meters, and the $\mathrm{d}I/\mathrm{d}V$ conductance curve (Fig. 4(c)) clearly shows that it is much more insulating than the tetragonal region, showing an asymmetric energy gap of 100–200 meV (Fig. 4(c)).

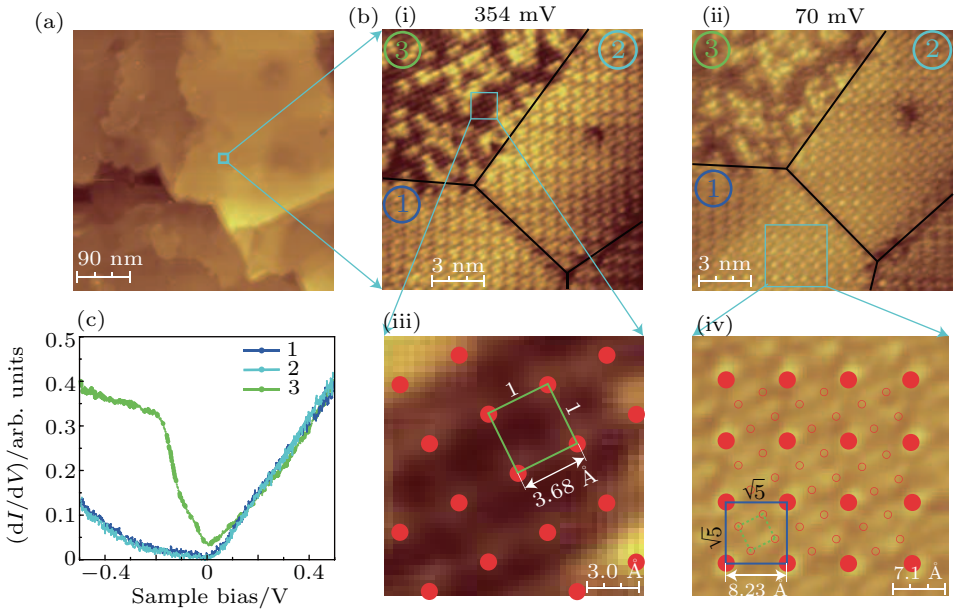

Fig. 4. Spatial inhomogeneity in FeS. (a) The topography image obtained by STM reveals flat terraces in FeS. (b) Zoomed-in topography scanned by STM at 354 mV (i) and 70 mV (ii) sample bias, respectively. Three coexisting regions are labeled. The details of region 3 in (i) and region 1 in (ii) are plotted in (iii) and (iv), respectively. The superimposed red dots in (iii) and (iv) indicate sulphur atoms' positions on the surface in 1×1 phase and $\sqrt{5} \times \sqrt{5}$ phase, respectively. The smaller red empty circles in (iv) are the guidance for eyes showing the position of sulphur atoms in the corresponding 1×1 phase. Colored squares indicate the smallest unit-cell found in each region. The size of each kind of unit-cell is labeled. (c) Typical $\mathrm{d}I/\mathrm{d}V$ curves from three different regions.

This observation is in consistent with the ARPES measurements (e.g., in Fig. 3(b)) as the insulating $\sqrt{5} \times \sqrt{5}$ domains naturally contribute less photocurrents than the metallic tetragonal regions, thus are one viable origin for the darker regions in the spatial map in Fig. 3(b) (other explanations to be explored include the residue and intermediate phases after the hydrothermal reaction). Also, this phase can further broaden the spectra of regular ARPES measurements in Figs. 2 and 3(d) due to the mixture of difference phases. The existence of the $\sqrt{5} \times \sqrt{5}$ phase not only makes it necessary to use spatially resolved experimental techniques in the investigation of FeS, but also suggests that prudent analysis is needed in the interpretation of macroscopic measurements on bulk crystals (e.g., electric transport, magnetoelectric effect, and quantum oscillations).

In summary, with combined STM and ARPES measurements, our work reveals the electronic band structure of the yet unexplored FeS, showing overall agreement with the *ab-initio* calculations. The similarity of FeS band structures to those of other Fe*X* compounds at their high temperature phases sets FeS an ideal and clean system to understand the mechanism of superconductivity in the iron chalcogenide family. Comparing with the non-superconducting FeTe with antiferromagnetic ground state, FeS does not hold any magnetic order, indicating that the magnetic order competes with superconductivity in FeSCs. In comparison with the superconducting FeSe, both the orthorhombic lattice distortion and the nematic order are absent in FeS, indicating the nematicity may enhances the superconducting temperature. In terms of the electronic structure, FeS bears the similar electronic structure with FeSe and $FeSe_{0.5}Te_{0.5}$ in the tetragonal phase, which both have several hole pockets at Γ and electron pockets at M, suggesting the inter-pocket electron–hole interaction is the main pairing mechanism in these compounds. The band renormalization in FeS is 2–3 for the hole-like bands, similar to that in $FeSe_{0.5}Te_{0.5}$, indicating the intermediate to strong corre-

lation level plays an important role in the superconductivity in FeSCs.[35–37] Further, the μ-ARPES and STM have clearly demonstrated the coexistence of 1×1 and $\sqrt{5} \times \sqrt{5}$ phases, showing the complexity of the material. Such observation is in agreement with formation of the insulating $\sqrt{5} \times \sqrt{5}$ phase in Se-rich FeSe multilayer films,[28] indicating they have the same origin. During the formation of the superstructure, the kinetic energy is reduced and the electronic correlation is enhanced, creating the insulating phase.

Supporting information

The supporting information includes: 1) details of the synthesis of the FeS crystal, 2) detailed information of STM experiment, 3) detailed information about the μ-ARPES experiment, 4) resolving bands with different orbitals in FeS, and 5) k_z dependence of the electronic structure of FeS.

Acknowledgments

Advanced Light Source is operated by Office of Basic Energy Science of US DOE (contract DE-AC02-05CH11231). We are also grateful for the beamtime at the Spectromicroscopy beamline, Elettra synchrotron; Beamline 5–4, SSRL, SLAC National Laboratory; Beamline 10.0.1, ALS, LBNL; BL I05, DLS and BL13U, NSRL.

References

[1] Lu D H, Yi M, Mo S K, Erickson A S, Analytis J, Chu J H, Singh D J, Hussain Z, Geballe T H, Fisher I R and Shen Z X 2008 *Nature* **455** 81

[2] Cruz C D L , Huang Q, Lynn J W, Li J, Ii W R, Zarestky J L, Mook H A, Chen G F, Luo J L, Wang N L and Dai P 2008 *Nature* **453** 899

[3] Yin Z P and Haule K G 2011 *Nat. Mater.* **10** 932

[4] Chubukov A 2012 *Annu. Rev. Condens. Matter Phys.* **3** 57

[5] Stewart G R 2011 *Rev. Mod. Phys.* **83** 1589

[6] Paglione J and Greene R L 2010 *Nat. Phys.* **6** 645

[7] Yi M, Liu Z K, Zhang Y, Yu R, Zhu J X, Lee J J, Moore R G, Schmitt F T, Li W, Riggs S, Chu J H, Lv B, Hu J, Hashimoto M, Mo S K, Hussain Z, Mao Z Q, Chu C W, Fisher I R, Si Q, Shen Z X and Lu D H 2015 *Nat. Commun.* **6** 7777

[8] Wang Q Y, Li Z, Zhang W H, Zhang Z C, Zhang J S, Li W, Ding H, Ou Y B, Deng P, Chang K, Wen J, Song C L, He K, Jia J F, Ji S H, Wang Y Y, Wang L L, Chen X, Ma X C and Xue Q K 2012 *Chin. Phys. Lett.* **29** 037402

[9] Zhang W H, Sun Y, Zhang J S, Li F S, Guo M H, Zhao Y F, Zhang H M, Peng J P, Xing Y, Wang H C, Takeshi F, Akihiko H, Li Z, Ding H, Tang C J, Wang M, Wang Q Y, He K, Ji S H, Chen X, Wang J F, Xia Z C, Li L, Wang Y Y, Wang J, Wang L L, Chen M W, Xue Q K and Ma X C 2014 *Chin. Phys. Lett.* **31** 017401

[10] Ge J F, Liu Z L, Liu C, Gao C L, Qian D, Xue Q K, Liu Y and Jia J F 2015 *Nat. Mater.* **14** 285

[11] Subedi A, Zhang L, Singh D J and Du M H 2008 *Phys. Rev. B* **78** 134514

[12] Ma F, Ji W, Hu J, Lu Z Y and Xiang T 2009 *Phys. Rev. Lett.* **102** 177003

[13] Jiang J, He C, Zhang Y, Xu M, Ge Q Q, Ye Z R, Chen F, Xie B P and Feng D L 2013 *Phys. Rev. B* **88** 115130

[14] Liu Z K, He R H, Lu D H, Yi M, Chen Y L, Hashimoto, M, Moore R G, Mo S K, Nowadnick E A, Hu J, Liu T J, Mao Z Q, Devereaux T P, Hussain Z and Shen Z X 2013 *Phys. Rev. Lett.* **110** 037003

[15] Bao W, Qiu Y, Huang Q, Green M A, Zajdel P, Fitzsimmons M R, Zhernenkov M, Chang S, Fang M, Qian B, Vehstedt E K, Yang J, Pham H M, Spinu L and Mao Z Q 2009 *Phys. Rev. Lett.* **102** 247001

[16] Hsu F C, Luo J Y, Yeh K W, Chen T K, Huang T W, Wu P M, Lee Y C, Huang Y L, Chu Y Y, Yan D C and Wu M K 2008 *Proc. Natl. Acad. Sci. USA* **105** 14262

[17] McQueen T M, Williams A J, Stephens P W, Tao J, Zhu Y, Ksenofontov V, Casper F, Felser C and Cava R J 2009 *Phys. Rev. Lett.* **103** 057002

[18] Margadonna S, Takabayashi Y, McDonald M T, Kasperkiewicz K, Mizuguchi Y, Takano Y, Fitch A N, Suard E and Prassides K 2008 *Chem. Commun.* **43** 5607

[19] Lai X F, Zhang H, Wang Y Q, Wang X, Zhang X, Lin J H and Huang F Q 2015 *J. Am. Chem. Soc.* **137** 10148

[20] Lin H, Li Y, Deng Q, Xing J, Liu J, Zhu X, Yang H and Wen H H 2016 *Phys. Rev. B* **93** 144505

[21] Boyd W C and Matsubara S 1962 *Science* **137** 669

[22] Denholme S J, Demura S, Okazaki H, Hara H, Deguchi K, Fujioka M, Ozaki T, Yamaguchi T, Takeya H and Takano Y 2014 *Mater. Chem. Phys.* **147** 50

[23] Denholme S J, Okazaki H, Demura S, Deguchi K, Fujioka M, Yamaguchi T, Takeya H, ElMassalami M, Fujiwara H, Wakita T, Yokoya T and Takano Y 2014 *Sci. Technol. Adv. Mater.* **15** 055007

[24] Pachmayr U, Fehn N and Johrendt D 2016 *Chem. Commun.* **52** 194

[25] Xing J, Lin H, Li Y, Li S, Zhu X, Yang H and Wen H H 2016 *Phys. Rev. B* **93** 104520

[26] Kirschner F K K, Lang F, Topping C V, Baker P J, Pratt F L, Wright S E, Woodruff D N, Clarke S J and Blundell S J 2016 *Phys. Rev. B* **94** 134509

[27] Yang X, Du Z, Du G, Gu Q, Lin H, Fang D, Yang H, Zhu X and Wen H H 2016 *Phys. Rev. B* **94** 024521

[28] Song C L, Wang Y L, Jiang Y P, Li Z, Wang L, He K, Chen X, Ma X C and Xue Q K 2011 *Phys. Rev. B* **84** 020503

[29] Song C L, Wang Y L, Jiang Y P, Wang L, He K, Chen X, Hoffman J E, Ma X C and Xue Q K 2012 *Phys. Rev. Lett.* **109** 137004

[30] Song C L, Wang Y L, Cheng P, Jiang Y P, Li W, Zhang T, Li Z, He K, Wang L, Jia J F, Hung H H, Wu C, Ma X, Chen X and Xue Q K 2011 *Science* **332** 1410

[31] Watashige T, Tsutsumi Y, Hanaguri T, Kohsaka Y, Kasahara S, Furusaki A, Sigrist M, Meingast C, Wolf T, Löhneysen H V, Shibauchi T and Matsuda Y 2015 *Phys. Rev. X* **5** 031022

[32] Wang X P, Richard P, Huang Y B, Miao H, Cevey L, Xu N, Sun Y J, Qian T, Xu Y M, Shi M, Hu J P, Dai X and Ding H 2012 *Phys. Rev. B* **85** 214518

[33] Yi M, Lu D, Chu J H, Analytis J G, Sorini A P, Kemper A F, Moritz B, Mo S K, Moore R G, Hashimoto M, Lee W S, Hussain Z, Devereaux T P, Fisher I R and Shen Z X 2011 *Proc. Natl. Acad. Sci. USA* **108** 6878

[34] Chen F, Zhou B, Zhang Y, Wei J, Ou H W, Zhao J F, He C, Ge Q Q, Arita M, Shimada K, Namatame H, Taniguchi M, Lu Z Y, Hu J, Cui X Y and Feng D L 2010 *Phys. Rev. B* **81** 014526

[35] Watson M D, Kim T K, Haghighirad A A, Davies N R, McCollam A, Narayanan A, Blake S F, Chen Y L, Ghannadzadeh S, Schofield A J, Hoesch M, Meingast C, Wolf T and Coldea A I 2015 *Phys. Rev. B* **91** 155106

[36] Watson M D, Kim T K, Haghighirad A A, Blake S F, Davies N R, Hoesch M, Wolf T and Coldea A I 2015 *Phys. Rev. B* **92** 121108

[37] Liu Z K, Yi M, Zhang Y, Hu J, Yu R, Zhu J X, He R H, Chen Y L, Hashimoto M, Moore R G, Mo S K, Hussain Z, Si Q, Mao Z Q, Lu D H and Shen Z X 2015 *Phys. Rev. B* **92** 235138

[38] Moreschini L, Lin P H, Lin C H, Ku W, Innocenti D, Chang Y J, Walter A L, Kim K S, Brouet V, Yeh K W, Wu M K, Rotenberg E, Bostwick A and Grioni M 2014 *Phys. Rev. Lett.* **112** 087602

[39] Zabolotnyy V B, Inosov D S, Evtushinsky D V, Koitzsch A, Kordyuk A A, Sun G L, Park J T, Haug D, Hinkov V, Boris A V, Lin C T, Knupfer M, Yaresko A N, Buchner B, Varykhalov A, Follath R and Borisenko S V 2009 *Nature* **457** 569